

LIF Measurements of the Cylindrical Hall Thruster Plume

IEPC-2009-137

*Presented at the 31st International Electric Propulsion Conference,
University of Michigan, Ann Arbor, Michigan, USA
September 20 – 24, 2009*

R. Spektor, K. D. Diamant, and E. J. Beiting

The Aerospace Corporation

Y. Raitses and N. J. Fisch

Princeton Plasma Physics Laboratory

This paper presents a Laser Induced Fluorescence (LIF) investigation of ion velocity profiles in the plume of the Fully Cylindrical Hall Thruster (FCHT) recently developed at the Princeton Plasma Physics Laboratory. These measurements confirm a previously measured $\sim 7\%$ increase in the exhaust velocity when the cathode keeper draws an excess current (overrun mode). Furthermore, it was found that velocity directions in the plume remain relatively unchanged for the cusped and direct magnetic field configuration in both overrun and non-overrun modes. It is shown that the reported plume narrowing in the overrun mode is due to the shift of the acceleration and ionization regions inward toward the anode. This conclusion is supported by the potential profiles extracted from the LIF measurements, which indicate that in the overrun mode a larger fraction of potential fall occurs inside the thruster. Recent probe measurements further substantiate these findings [Raitses *et al.*, *Phys. Plasma* 16, 057106 (2009)]. The ratio of the potential fall experienced by ions inside the thruster over the actual potential drop within the thruster increases from 20% in the non-overrun regime with magnets in the direct configuration to 70% in the overrun mode with magnets in the cusped configuration. Magnetic field lines outside the thruster channel are found to be *not* equipotential, with the degree of equipotentiality gradually increasing at the thruster exit toward the edge.

I. Introduction

Annular Hall thrusters have been extensively developed in the power range from approximately 0.5 to 5 kW with specific impulse from about 1500 to 2000 s and total efficiency from 45 to 55%. A number of methodologies are available for scaling Hall thrusters to power levels below a few hundred watts while attempting to preserve specific impulse and efficiency.¹⁻⁶ All face the same challenges created by the need to reduce channel size to preserve ionization efficiency. Small size leads to difficulty in generation of magnetic fields with appropriate magnitude and topology and to increased particle losses with consequent increases in electron transport, heating, erosion, and plume divergence,^{7,8} and therefore reduced efficiency, specific impulse, and life.

Raitses and Fisch developed a Cylindrical Hall Thruster (CHT), featuring a reduced surface-to-volume ratio and unique magnetic topology.⁹ The central magnetic pole and inner ceramic of the CHT are shortened thus producing an annular region near the anode, which is followed by a cylindrical region. Ion acceleration occurs mainly in the low surface-to-volume cylindrical region resulting in reduced particle losses.^{10,11} Electrons are confined in the annular region by the mainly radial magnetic field, as in conventional annular Hall thrusters. The magnetic field in the cylindrical region has both a substantial axial component and a large axial gradient so that electron confinement occurs by magnetic mirroring near the annular part of the

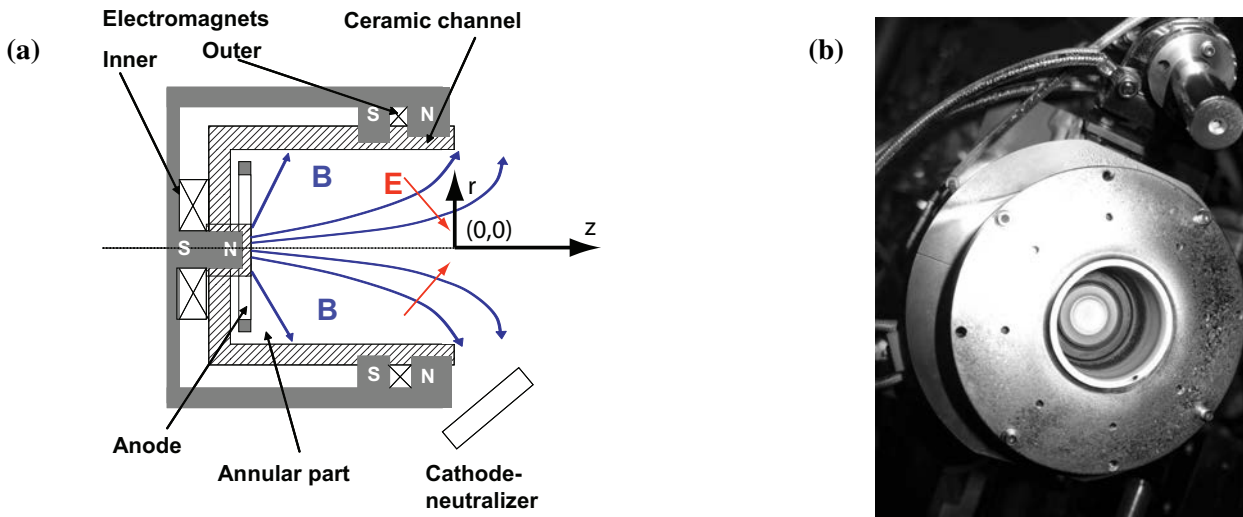


Figure 1. Schematic of the FCHT thruster in the direct configuration, panel (a), and a picture of the FCHT with the HWPES-250 cathode, panel (b).

channel and by the adverse potential gradient on the cathode side.¹² The CHT exhibits low discharge current oscillations¹⁰ and high ionization efficiency.¹³ For normal thruster operation the plume divergence is large, but by “overrunning” the discharge current in 2.6 and 3 cm diameter CHTs, the divergence is reduced by 20-30% and the ion energy distribution is shifted to higher energies.¹⁴ The overrun regime is attained by running a current to the keeper of the hollow cathode. Anode efficiencies of 33-41% (not including power required to overrun the discharge) at 50-175 W were measured with the 2.6 cm thruster.¹⁴

A recent study¹⁵ confirmed the plume narrowing and performance enhancement in the overrun regime for a 3 cm diameter CHT. Plume divergence (half angle containing 90% of the total ion current) was observed to decrease from 71° to 53°, primary ion peak energies increased by 9% with fewer primary ions at high angles, and anode efficiencies (not including overrun power) of 20-38% were measured at 75-190 W. Very similar results were obtained when the CHT was modified to remove the annular region (i.e. the inner channel wall ends flush with the anode downstream face), producing a fully cylindrical thruster (FCHT), as shown in Fig. 1.

The underlying physical processes responsible for the enhanced performance in the overrun regime are not fully understood. Recent probe measurements showed that the voltage potential drop inside the channel increases in the overrun regime.¹⁶ It was suggested that this contributes to the plume narrowing. In this paper we use a non-invasive diagnostic to investigate these reported improvements through a series of comparisons between the ion velocity distributions in various thruster operating regimes. Specifically, we focus our attention on the FCHT configuration, and study the differences between the overrun and the non-overrun modes both with the direct and cusped magnetic topologies. In the direct configuration, shown in Fig. 1(a), the inner and outer magnet poles have the same polarity sense, and in the cusped configuration the outer magnet polarity is reversed. We use the Laser Induced Fluorescence (LIF) technique to map ion velocities in the plume and infer electric fields for all four permutations of magnetic fields and current overrun regimes. The rest of the paper is organized as follows. The setup of the laser induced fluorescence apparatus is described in Section II. Section III presents experimental results and discusses our findings. We conclude with final remarks in Section IV.

II. Experimental Setup

The experiments were performed in the Near Field Facility (NFF) at The Aerospace Corporation. The facility comprises a 3 m long and 1.5 m diameter stainless steel chamber pumped by two He-cooled nude sails with the speed of 42,000 l/s. The system is capable of maintaining a base pressure of 6.7×10^{-5} Pa; this increases to as much as 9.3×10^{-4} Pa (adjusted for Xe) with a thruster operating. All pressures were measured with an ionization gauge mounted on the side of the chamber next to the thruster. A detailed description of the NFF chamber is given in Ref. 17.

The FCHT, shown in Fig. 1, consists of a boron-nitride ceramic channel, an annular anode, which also acts as the gas distributor, two electromagnet coils, and a magnetic core. The channel is 3 cm in diameter and the thruster exit is located 22 mm from the anode. The magnet coils were run in either a “direct” configuration, which produced an enhanced axial component of the magnetic field at the outer wall and a stronger magnetic mirror on the thruster axis¹⁸ or in the “cusped” configuration in which the outer magnet polarity is reversed. A commercial hollow cathode (Heatwave Labs model HWPES-250) supplied electrons to the discharge and plume. The cathode keeper exit aperture was located 54 mm radially from thruster centerline, and 20 mm downstream of the thruster exit plane. The angle between the thruster and cathode axes was approximately 40°.

Figure 1(b) is a photograph of the FCHT thruster in this configuration. For the experiments described here we operated the thruster with the discharge voltage of 250 V and current near 0.6 A. Magnetic field was established by supplying 2 A to the inner coil and 1.5 A to the outer coil in both direct and cusped configurations. Furthermore, we operated the thruster in two discharge modes. Throughout this paper we refer to these modes as the “overrun” mode in which the cathode keeper was drawing 3 A of current, and the “non-overrun” mode, where the keeper did not draw any current.

The thruster was placed on a motorized platform that could be translated in three orthogonal directions; its exhaust was directed toward the helium-cooled sails. This platform allowed us to perform spatially

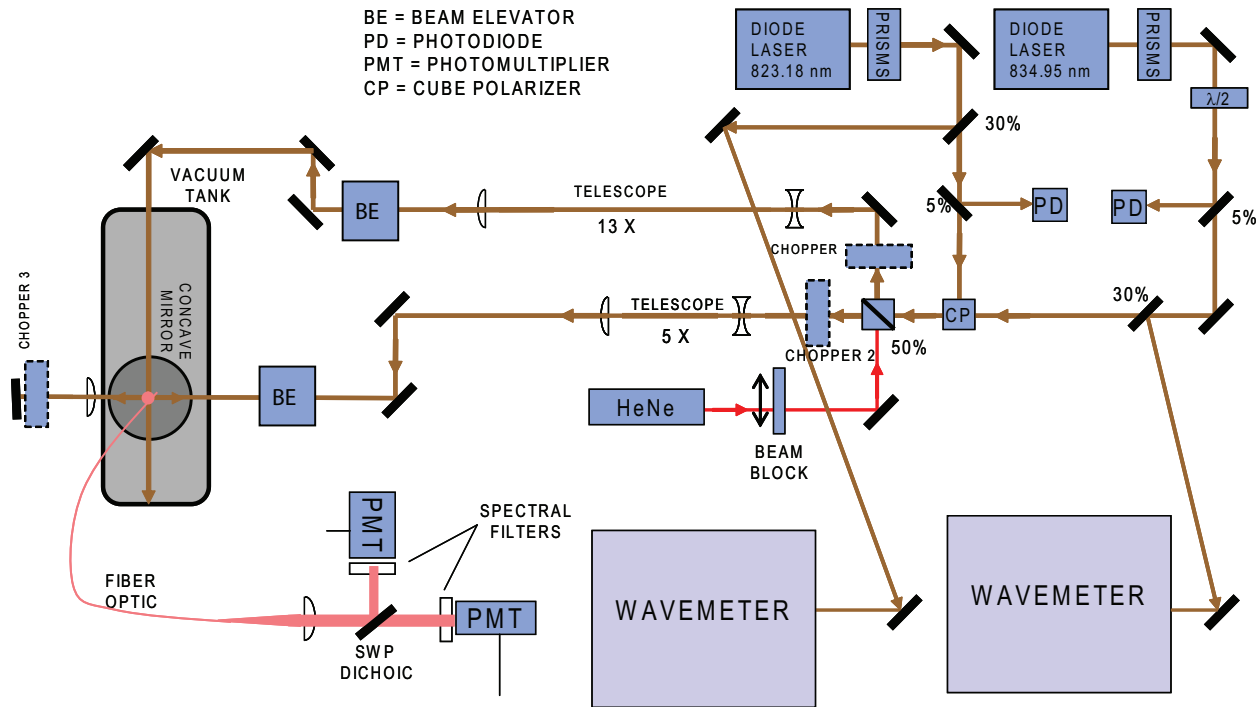


Figure 2. Schematic of the LIF setup used for the FCHT measurements.

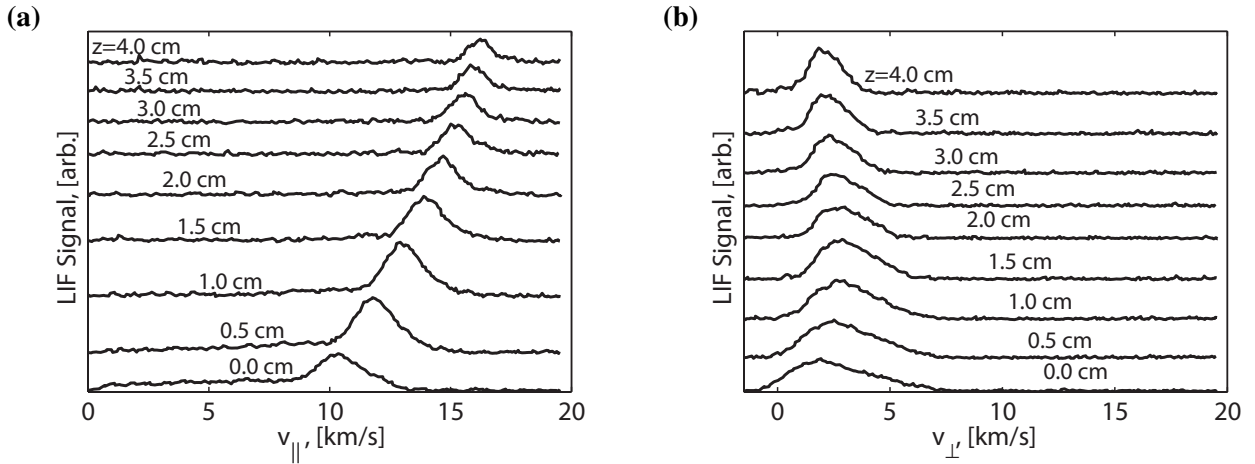


Figure 3. Evolution of Xe^+ velocity distribution as a function of distance from the thruster exit at $r = 1 \text{ cm}$. The thruster was operated in the cusp configuration in the non-override mode. Panel (a) shows the axial velocity component, and Panel (b) shows the transverse velocity component.

resolved measurements in the plume by moving the thruster relative to a stationary external collection optics and the LIF apparatus. Using the platform we performed the LIF measurements in the near field of the thruster plume. The data were collected in the region spanning the thruster exit up to 4.0 cm along z direction, and from the thruster centerline up to 3.0 cm along the radial direction, with the thruster exit at the centerline being the origin, as shown in Fig. 1(a).

The LIF instrument shown in Fig. 2 was designed to measure two dimensional (z, r) velocity profiles of Xe ion and neutral species simultaneously. It is an expanded version of the apparatus previously used to investigate the SPT-140 thruster.^{19,20} This paper presents only the data collected using the Xe^+ portion of the setup. Here a 6000 series New Focus tunable diode laser with the center vacuum wavelength of 834.95 nm (driven by a Vortex controller) excited the $5d^4F_{5/2} - 6p^4D_{5/2}$ transition in Xe^+ . The laser beam was divided into two components, each of which was sent through a series of mirrors and a telescope to cross orthogonally in the NFF vacuum chamber. One beam entered the end of the chamber and measured the axial component of ion velocity; the other entered the side and measured the transverse component. The transverse beam was reflected from an external mirror and refocused onto the crossing point of the transverse and axial beams. The forward and reflected transverse signals provided a reliable zero-velocity reference and verified the wavemeter measurements. Each of the three beams was chopped at a different frequency. A He-Ne and a green diode (not shown in Fig. 2) lasers aided alignment.

The LIF signal from the $6p^4D_{5/2} - 6s^4P_{3/2}$ Xe^+ transition at 532 nm was collected by a 15 cm concave mirror and focused onto a 2 mm diameter fiber optic bundle, as described in Ref. 17. A lens installed near the fiber optic bundle improved the signal-to-noise ratio. The light exiting the fiber optic bundle passed through a 10 nm bandwidth interference filter and was focused on a photomultiplier tube. The electrical signal was divided among three Stanford Research SR830 lock-in amplifiers, each tuned to one of the three chopper frequencies. A Burleigh WA-1500 wavemeter measured the laser wavelength during the laser sweeps. This scheme allowed the simultaneous measurements of both components of the Xe ion velocity distribution function.

The data collected by scanning the diode laser corresponded to Doppler-shifted Xe ion transition energies. Each scan consisted of approximately 300 data points and typically covered a frequency range of 40 GHz. Figure 3 displays a typical data set of the axial (panel a) and transverse (panel b) ion velocity distributions at various axial positions. Here $r = 1 \text{ cm}$ and the thruster is running in the non-override mode with the magnetic coils in the cusped configuration. Each trace in Fig. 3 is a single 6 minute scan. At a few locations where the LIF signal-to-noise ratio was lower we collected up to three scans to reduce measurement

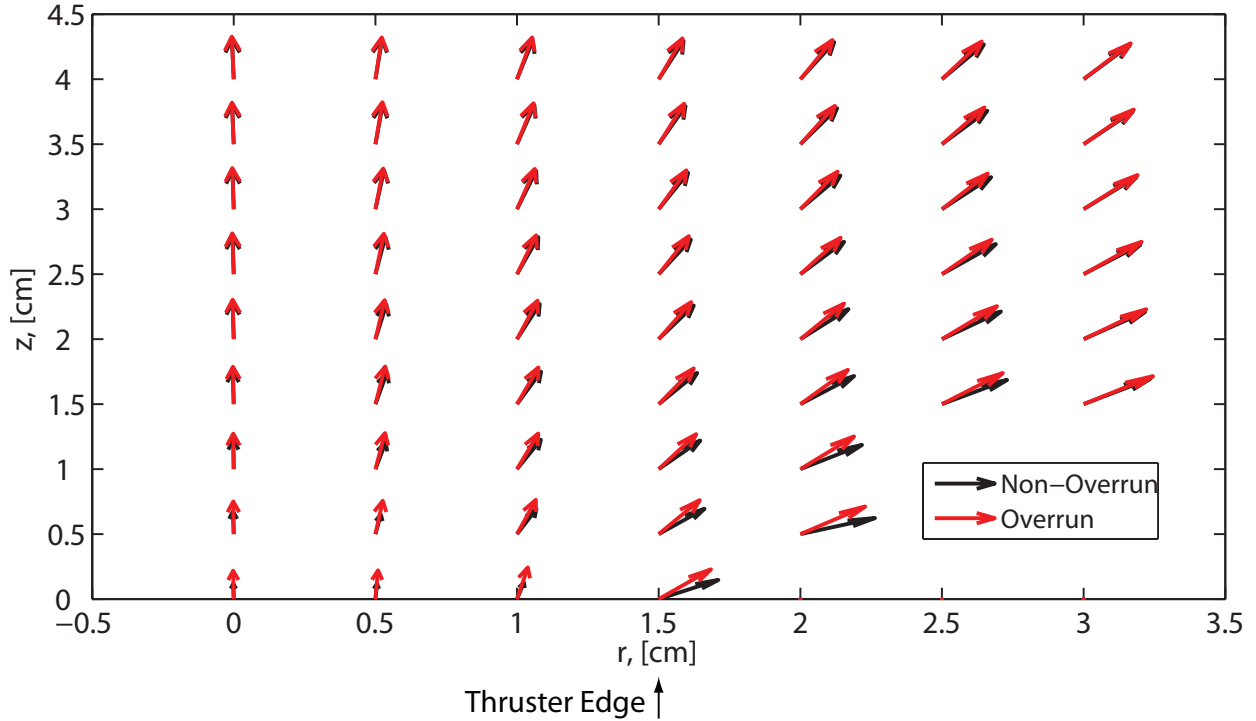


Figure 4. Ion velocity divergence profile in the plume of the FCHT thruster in the direct configuration. The non-overrun case is shown by black arrows, while the overrun case is shown by red arrows.

uncertainty.

III. Results and Discussion

Figure 4 shows a two-dimensional ion velocity vector map, which we obtained from the LIF measurements with the thruster running in the direct magnetic field configuration. Velocity vectors were determined from the maxima of the velocity distributions. The figure shows the velocity vector map with the thruster running in the keeper-off (‘non-overrun’) configuration indicated by black arrows and keeper drawing 3 A in the overrun configuration, which is marked by red arrows. The velocity vector maps for the thruster running in the cusped magnetic field configuration in both overrun and non-overrun modes look very similar to the maps shown in Fig. 4. It is clear from this map that the velocity divergence is similar for the overrun and non-overrun cases.

Figure 5(a) shows the axial component of ion velocity along the centerline for the non-overrun and overrun cases with both magnetic field profiles. These data indicate that overrunning the cathode is beneficial. In both cusped and direct configurations the LIF data shows $\sim 7\%$ increase in the ultimate exhaust velocity over that in the corresponding non-overrun cases. Similar findings from the probe measurements have been reported for the direct magnetic field configuration.¹⁵ The greatest difference in ion velocities among various thruster operating regimes appears at the thruster exit plane. For the cusped configuration with the keeper drawing a current of 3 A the ion exhaust velocity at the thruster exit (at the centerline) is almost 30% greater than that with the keeper off. The difference is more dramatic for the direct configuration where the overrun case shows that ion velocity at the thruster exit is almost double that in the non-overrun case. Furthermore, the measurements show that in the non-overrun regime a significant portion of ion acceleration (up to half in the direct configuration) occurs outside of the thruster channel. We, therefore, conclude that

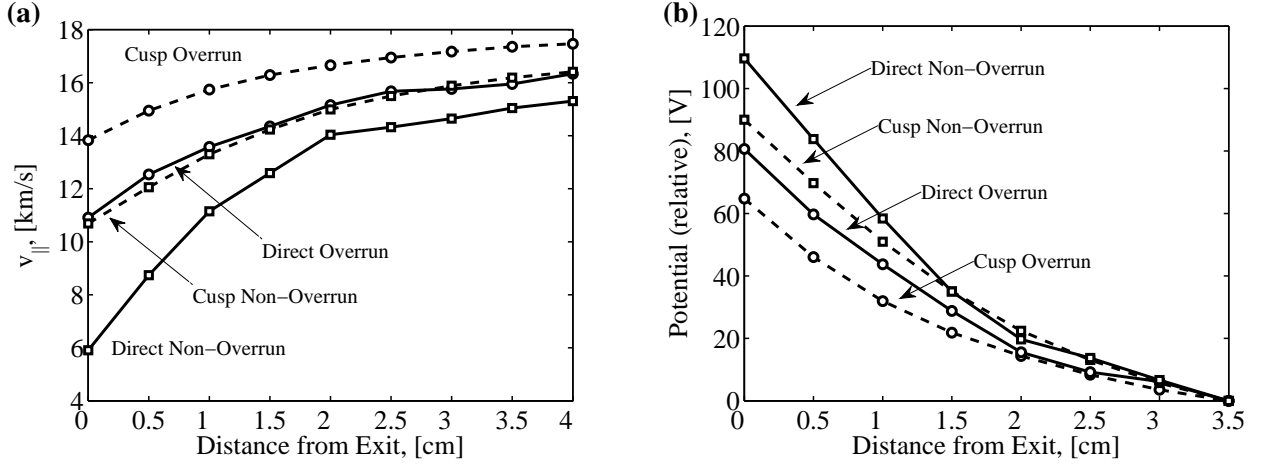


Figure 5. Panel (a) shows centerline velocity profiles for the four studied regimes. Solid lines represent direct magnet configuration, while dashed lines represent cusped configuration. Squares designate the non-overrun condition, while circles stand for the overrun cases. Panel (b) shows relative potential profiles along the centerline in the FCHT plume for the same four modes shown in panel (a).

in the overrun regime the acceleration region is located closer to the anode than in the non-overrun regime.

As noted, Fig. 4 shows that there is almost no change in the velocity divergence profile between the overrun and non-overrun regimes of operation. Flux probe measurements, however indicate significant plume reduction in the overrun case.^{14,15} These two observations can be reconciled if the ionization region in the overrun regime is nearer the anode than in the non-overrun regime. Thus, in the overrun regime more ions are produced deeper within the thruster and follow less divergent trajectories resulting in the observed plume reduction. These conclusions are further supported by recently published probe measurements of plasma potential profiles.¹⁶

We can estimate electric fields and potential falls from the measured ion velocity profiles. This is done using the fluid momentum conservation equation,²¹

$$n_i m_i \frac{\partial}{\partial t} \vec{v}_i + n_i m_i (\vec{v}_i \cdot \nabla) \vec{v}_i - n_i e (\vec{E} + \vec{v}_i \times \vec{B}) + \nabla \cdot \vec{P}_i = \vec{R}_{col}, \quad (1)$$

where n_i , m_i , and v_i are the ion density, mass, and velocity respectively, \vec{E} and \vec{B} are electric and magnetic fields, \vec{P}_i is the pressure tensor, and \vec{R}_{col} is the collision term. In the following analysis we assume the steady-state condition and that ions are collisionless, cold, and unmagnetized. These assumptions allow us to express electric field directly from the velocity components as

$$\begin{aligned} E_x &= \frac{m_i}{e} \left(v_i^x \frac{\partial v_i^x}{\partial x} + v_i^y \frac{\partial v_i^x}{\partial y} \right), \\ E_y &= \frac{m_i}{e} \left(v_i^x \frac{\partial v_i^y}{\partial x} + v_i^y \frac{\partial v_i^y}{\partial y} \right). \end{aligned} \quad (2)$$

The above expression for electric field is strictly valid only if the fluid velocities represent the velocity-distribution-weighted velocity average ($\vec{v}_i = \int \vec{v} f(\vec{v}) \partial \vec{v}$). A better approach for computing the fields would be to use the Boltzmann equation with the measured velocity distribution functions directly. In order to simplify our calculations, however, we approximated the fluid velocities by the maxima of the velocity distributions. For the cases where the distribution is Gaussian (or otherwise symmetric) the peak will correspond to the average velocity. On the other hand, such an estimate from an asymmetric distribution function will result in an error. Typical transverse and parallel velocity distribution functions obtained from the LIF

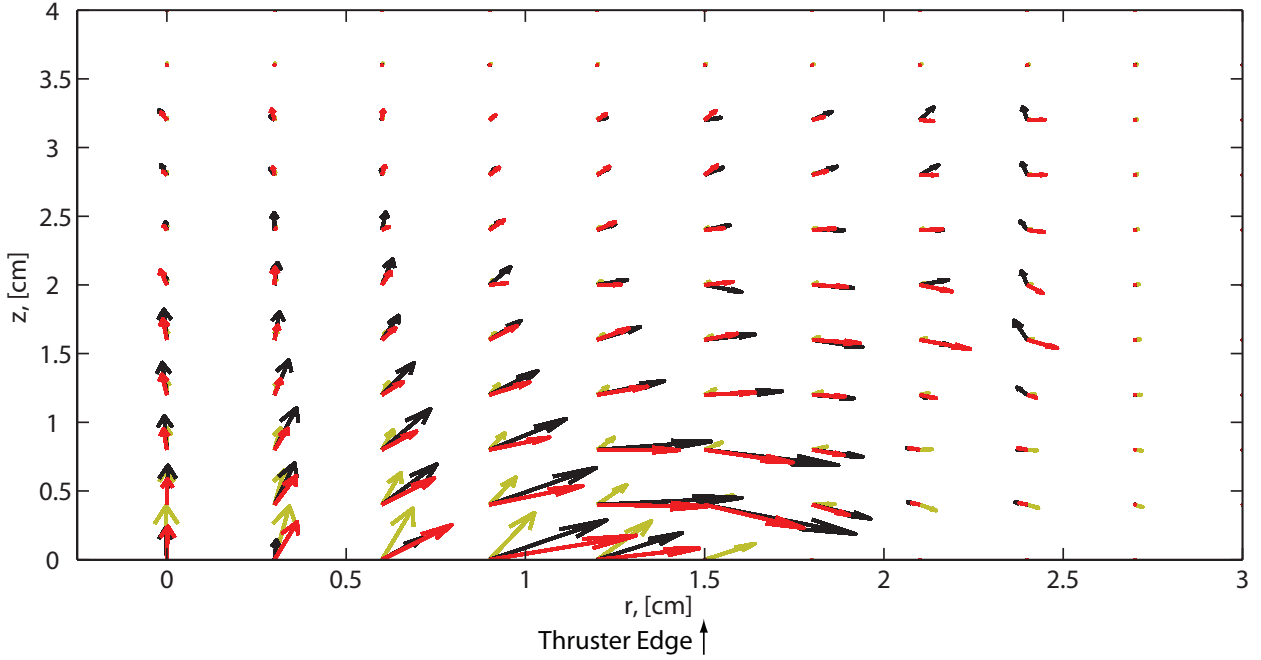


Figure 6. Measured magnetic and calculated electric field profiles in the plume of the FCHT thruster. Green arrows indicate magnetic field vectors. Red arrows designate electric field vectors in the overrun regime and black arrows show the non-overrun mode.

measurements are shown in Fig. 3. These data indicate that the velocity distributions are largely symmetric. The greatest asymmetry occurs at the thruster exit, where the perpendicular and parallel components of velocity exhibit high-velocity and low-velocity tails respectively.

Figure 5(b) shows the centerline potential profiles for the regimes derived from the velocity measurements shown in Fig. 5(a). Here we have arbitrarily assigned $U = 0$ at $z = 3.5 \text{ cm}$ for all thruster regimes. This is a valid assumption because the ion velocities plateau near $z = 3.5 \text{ cm}$, so the underestimate in the potential measurement is likely small. Figure 6 shows an electric field vector map for both overrun and non-overrun regimes of thruster operation in the direct magnetic field configuration. The black arrows correspond to the non-overrun condition, while the red arrows correspond to the overrun case. Once again, the cusp profiles, which are not shown, look very similar. Juxtaposed on top of the electric field is the measured magnetic field vector map (green arrows).

We now define the potential utilization parameter, η_U , as the ratio of the potential fall inside the thruster experienced by the accelerated ions, U_i , over the potential computed by subtracting the potential fall in the plume, U_p from the applied discharge voltage, U_d ,

$$\eta_U = \frac{U_i}{U_d - U_p} = \frac{0.5m_i v_{exit}^2}{250 \text{ V} - 0.5m_i v_{ult}^2}, \quad (3)$$

where v_{exit} and v_{ult} are the ion exit and ultimate exhaust velocities. This ratio is an indicator of acceleration effectiveness within the thruster, with a value of unity indicating all of the potential drop couples into ion acceleration.

Table 1. Potential utilization parameter

	Direct Non-Overrun	Cusp Non-Overrun	Direct Overrun	Cusp Overrun
Potential Utilization Parameter	0.2	0.5	0.5	0.7

We compute η_U using the centerline velocity values. Table 1 lists the calculated values for all four thruster configurations. The cusped overrun configuration shows the highest utilization fraction, while the direct non-overrun configuration shows the least efficient utilization. These numbers confirm that not only does the peak gradient in the electric field moves inward in the overrun mode, as shown in Fig. 5(b), but the ionization region also moves toward the anode. Recent RPA measurements further support that conclusion.¹⁴ They show that in the overrun regime the peak of the ion energy distribution shifts to higher values, indicating that ions are born at a higher potential. Thus, inside the thruster ions are accelerated by a larger fraction of the available potential fall in the overrun mode than in the non-overrun mode.

From the electric field vector maps we can also determine the degree of magnetic line equipotentiality. When electrons are magnetized and in the absence of electron pressure gradient we expect the potential along a magnetic line to remain relatively unchanged. In such a case we expect the electric field to be orthogonal to the magnetic field lines. Although it is most interesting to investigate this field behavior in the ion acceleration region, we can glean information about internal field behavior from our plume measurements. Our results show that at the centerline and outside of the thruster channel the fields are not equipotential because both electric and magnetic fields are co-aligned. On the other hand, following the magnetic line that intersects the thruster lip (see Fig. 1(a)) we see a greater degree of equipotentiality at the edge of the thruster exit plane. Figure 6 shows this behavior. In particular it demonstrates that at the thruster exit plane magnetic lines are not equipotential, as indicated by the shallow angle between the magnetic and electric fields. Along the centerline the magnetic and electric fields are co-aligned and toward the edge of the thruster ($r = 1.5 \text{ cm}$) the fields become more orthogonal, indicating a greater degree of equipotentiality. Furthermore, in the overrun case (red arrows) the magnetic and electric fields are closer to orthogonal than those in the non-overrun case.

IV. Conclusions

In this paper we reported on the Xe^+ LIF measurements in the plume of the FCHT thruster. The measurements were performed with the thruster operating in the overrun and non-overrun modes as well as with magnetic fields in the direct and cusped configurations. We found that the ultimate exhaust velocity increases by approximately 7% in the overrun regime for both magnetic field configurations. The overrun regime in the cusped magnetic field configuration resulted in the highest ultimate exhaust velocity (17 km/s) for all four modes that we studied. Surprisingly, velocity vector map showed that there is very little difference in the ion velocity direction between all four modes. This implied that the observed plume narrowing in the overrun mode is due to the shift in the location of the ionization and acceleration regions toward the anode.

Potential profiles extracted from the velocity measurements indicated that in the overrun regime a larger portion of the potential fall occurred inside the thruster. This led to a calculation of the potential utilization parameter. We showed that in the cusped overrun regime the potential utilization reaches 70% while in the direct non-overrun regime the utilization drops to 20%.

Finally, we found that the magnetic field lines outside the thruster are not equipotential. The degree of equipotentiality outside the thruster increased closer to the thruster exit and toward the channel edge. Furthermore, the degree of equipotentiality is greater in the overrun regime. This implies that in the overrun regime electron transport across magnetic lines is inhibited, a conclusion that is also supported by probe measurements.¹⁶ Because electron transport reduction produces thruster efficiency improvement, this finding merits further investigation.

Acknowledgements

The authors thank Dr. Artem Smirnov for fruitful discussions. The project was supported by The Aerospace Corporation through its Independent Research and Development Program.

All trademarks, service marks, and trade names are the property of their respective owners.

References

- ¹V. Khayms and M. Martinez-Sanchez. Design of a miniaturized Hall thruster for microsattellites. Presented at the 32nd IAIAA/ASME/SAE/ASEE Joint Propulsion Conference, Lake Buena Vista, FL, 1-3, July, 1996, AIAA-1996-3291.
- ²V. Hruby, J. Monheiser, B. Pote, P. Rostler, J. Kolencik, and C. Freeman. Development of low power Hall thrusters. Presented at the 30th Plasmadynamics and Lasers Conference, Norfolk, VA, 28 June - 1 July, 1999, AIAA-1999-3534.
- ³N.Z. Warner and M. Martinez-Sanchez. Design and preliminary testing of a miniaturized tal Hall thruster. Presented at the 42nd AIAA/ASME/SAE/ASEE Joint Propulsion Conference (JPC), Sacramento, CA, 9-12 July 2006, AIAA-2006-4994.
- ⁴F. Battista, E. DeMarco, T. Misuri, and M. Andrenucci. A review of the Hall thruster scaling methodology. Presented at the 30th International Electric Propulsion Conference, Florence, Italy, 17-20 September 2007, IEPC-2007-313.
- ⁵M. Belikov, O. Gorshkov, E. Dyshlyuk, A. Lovtsov, and A. Shagayda. Development of low-power Hall thruster with lifetime up to 3000 hours. Presented at the 30th International Electric Propulsion Conference, Florence, Italy, 17-20 September 2007, IEPC-2007-129.
- ⁶E. Ahedo and J Gallardo. Scaling down Hall thrusters. Presented at the 28th International Electric Propulsion Conference, Toulouse, France, 17-20 March 2003, IEPC-2003-104.
- ⁷M. Belikov, O. Gorshkov, V. Muravlev, R. Rizakhanov, A. Shagayda, and A. Shnirev. Hall-type low- and mean-power thrusters output parameters. Presented at the 35th AIAA/ASME/SAE/ASEE Joint Propulsion Conference (JPC), Los Angeles, CA, 20-24 June 1999, AIAA-1999-2571.
- ⁸M. Belikov, O. Gorshkov, V. Muravlev, R. Rizakhanov, A. Shagayda, and A. Shnirev. High-performance low power Hall thruster. Presented at the 37th AIAA/ASME/SAE/ASEE Joint Propulsion Conference (JPC), Salt Lake City, UT, 8-11 July 2001, AIAA-2001-3780.
- ⁹Y. Raitses, N.J. Fisch, K.M. Ertmer, and C.A. Burlingame. A study of cylindrical Hall thruster for low power space applications. Presented at the 36th AIAA/ASME/SAE/ASEE Joint Propulsion Conference, Huntsville, AL, July 2000, AIAA-2000-3421.
- ¹⁰Y. Raitses and N. J. Fisch. Parametric investigations of a nonconventional Hall thruster. *Phys. Plasmas*, 8(5):2579, May 2001.
- ¹¹A. Smirnov, Y. Raitses, and N. J. Fisch. Plasma measurements in a 100 w cylindrical Hall thruster. *J. Appl. Phys.*, 95(5):2283, March 2004.
- ¹²A. Smirnov, Y. Raitses, and N.J. Fisch. Experimental and theoretical studies of cylindrical Hall thrusters. *Phys. Plasmas*, page 057106, 2007.
- ¹³A. Smirnov, Y. Raitses, and N. J. Fisch. Enhanced ionization in the cylindrical Hall thruster. *J. Appl. Phys.*, 94(2):852, July 2003.
- ¹⁴Y. Raitses, A. Smirnov, and N.J. Fisch. Enhanced performance of cylindrical Hall thrusters. *Applied Phys. Let.*, 90:221502, 2007.
- ¹⁵K. D. Diamant, J. E. Pollard, Y. Raitses, and N. J. Fisch. Low power cylindrical Hall thruster performance and plume properties. Presented at the 44th AIAA/ASME/SAE/ASEE Joint Propulsion Conference, Hartford, CT, July 21-23, 2008, AIAA-2008-4998.
- ¹⁶Y. Raitses, A. Smirnov, and N. J. Fisch. Effects of enhanced cathode electron emission on hall thruster operation. *Phys. plasmas*, 16:057106, 2009.
- ¹⁷R. Spektor and E. J. Beiting. Non-invasive plasma diagnostic inside a Hall thruster discharge. Presented at the 30th International Electric Propulsion Conference (IEPC), Florence, Italy Sep. 17–20, 2007. IEPC-2007-69.
- ¹⁸A. Smirnov, Y. Raitses, and N. J. Fisch. The effect of magnetic field on the performance of low-power cylindrical Hall thrusters. Presented at the 29th International Electric Propulsion Conference, Princeton University, Princeton, NJ, October 31 - November 4, 2005, IEPC-2005-099.
- ¹⁹E.J. Beiting and J.E. Pollard. Measurements of xenon ion velocities of the SPT-140 using laser induced fluorescence. Presented at the 3rd International Conference of Spacecraft Propulsion, Cannes, France, October 10–13, 2000.
- ²⁰J.E. Pollard and E.J. Beiting. Ion energy, ion velocity, and thrust vector measurements for the SPT-140 Hall thruster. Presented at the 3rd International Conference of Spacecraft Propulsion, Cannes, France, October 10–13, 2000.
- ²¹N. K. Krall and A.W. Trivelpiece. *Principles of plasma physics*. McGraw-Hill Book Company, New York, 1973.